Article

Impurity Combination Effect on Oxygen Absorption in α_2-Ti$_3$Al

Alexander V. Bakulin [1,*], Lora S. Chumakova [1], Sergey O. Kasparyan [1] and Svetlana E. Kulkova [1,2]

[1] Institute of Strength Physics and Materials Science, Siberian Branch of Russian Academy of Sciences, pr. Akademichesky 2/4, 634055 Tomsk, Russia; chumakova.lora@mail.ru (L.S.C.); kasparyan@ispms.ru (S.O.K.); kulkova@ms.tsc.ru (S.E.K.)

[2] Physics Department, National Research Tomsk State University, pr. Lenina 36, 634050 Tomsk, Russia

* Correspondence: bakulin@ispms.tsc.ru; Tel.: +7-3822-286-952

Abstract: The effect of substitutional impurities of the transition metals of VB–VIIB groups on the oxygen absorption in the doped α_2-Ti$_3$Al alloy was studied by the projector-augmented wave method within the density functional theory. It is established that all considered impurities prefer to substitute for a Ti atom rather than an Al atom. Changes in the absorption energy due to impurities being in the first neighbors of the oxygen atom were estimated. It was demonstrated that the doping resulted in a decrease in the oxygen absorption energy, which is mainly caused by the chemical contribution to it. The interaction energy between impurity atoms was calculated in the dependence on the interatomic distance. It was shown that the configuration with the impurity atoms being in the second neighbors of each other was stable in comparison with other possible configurations. The influence of two impurity atoms being in the first neighbors of oxygen is additively enhanced. It was revealed that the effect of two impurity atoms on the oxygen absorption energy can be estimated as the sum of the effects of separate impurities with an accuracy of more than ~90%.

Keywords: oxygen; absorption; impurity effect; Ti$_3$Al alloy; first principles calculations

1. Introduction

Intermetallic alloys based on titanium and aluminum are known to be characterized by their low densities, high specific strength and stiffness, and high creep resistance under moderately elevated temperatures [1–5], which makes them ideal materials for various high-temperature structural applications in automobile, aerospace, and gas turbine industries [6–8]. Two of the most promising intermetallic phases of the binary system Ti–Al for technical applications are α_2-Ti$_3$Al and γ-TiAl. These materials are considered to be excellent for manufacturing static components or rotating parts [3,4,6,9]. At the same time, the Ti$_3$Al alloy has a specific modulus and stress rupture resistance comparable to that of the superalloys; however, the complete absence of room temperature plasticity posed the primary challenge in using it as a structural material. Moreover, the single γ-phase TiAl alloy is brittle with practically no deformability at temperatures up to ~1000 K [1,6]. At high temperature, mixed oxide scales grow by the competitive oxidation of Ti and Al, which prevents the formation of a continuous and dense α-alumina [10–14].

Two-phase TiAl/Ti$_3$Al lamellar alloys possess a number of properties that distinguish them from the TiAl and Ti$_3$Al constituent single-phase alloys. For example, toughness, fatigue and creep resistance, and other properties are appreciably improved [15–18]. It is demonstrated that the minimum creep rate of two-phase lamellar alloys is up to an order of magnitude lower than the creep rates of the constituent single-phase alloys [19,20]. In fully lamellar structures, a very low dislocation activity and almost no twinning structures are observed [21]. At the same time, the high-temperature corrosion resistance of the two-phase lamellar alloys is still insufficient.

The addition of some alloying elements can enhance both the oxidation resistance and mechanical properties of single-phase TiAl and Ti_3Al and two-phase lamellar TiAl/Ti_3Al alloys. For example, an addition of V, Cr, Nb, Mo, Ta, and W produces solid solution strengthening (see [1,6,22–26] and references therein). The latter is also advantageous for the creep resistance. The Nb, Mo, Ta, and W elements are very effective in improving oxidation resistance [1,6,27–31], while the addition of Cr or V does not improve it [29]. It is a reason why almost all multicomponent alloys contain at least 2 at.% Nb, which is found to be the most appropriate.

In several papers [32–35], the energetics of substitutional defect formation in the α_2-Ti_3Al and γ-TiAl alloys was investigated by experimental and theoretical methods. Summing up the obtained results, it is possible to conclude that the energy-preferable situation is if V, Cr, Nb, Mo, Ta, W, and Re atoms occupy the Ti sublattice in the Ti_3Al alloy. In our earlier papers [36–38], the oxygen diffusion properties in both γ-TiAl and α_2-Ti_3Al alloys were investigated. It was established that the highest absorption energy corresponded to the positions with the highest number of Ti atoms in the nearest neighbors. The key migration barrier is connected with a jump from these sites to the nearest tetrahedral sites. In the paper [38], the impurity influence on the temperature-dependent diffusion coefficient in the Ti_3Al alloy was investigated. It was concluded that the dominant factor determining the change in the diffusion coefficient upon doping is a change in the oxygen absorption energy. Note that in [38], only the influence of single impurity atom on the absorption and migration energies was considered. At the same time, real alloys are multicomponent ones and the influence of several dopants on the absorption energy is desirable to be known.

Thus, the main goal of the present paper is to study the influence of an increase of impurity concentration or the addition of other impurities on the oxygen absorption in the α_2-Ti_3Al alloy. The increase in the concentration of impurity atoms leads to oxygen interaction with two dopant atoms simultaneously and makes the absorption process more complicated. The transition metals of VB–VIIB groups, such as V, Cr, Nb, Mo, Ta, W, and Re, are considered because of their favorable effect on the corrosion resistance or the mechanical properties of the alloy.

2. Computational Details

First-principles calculations of the alloy electronic structure were performed by the plane-wave basis projector-augmented wave (PAW) method [39,40] implemented by VASP (The Vienna Ab initio Simulation Package) code [41–43]. The generalized gradient approximation for an exchange-correlation functional in the PBE form [44] was used. It should be noted that the α_2-Ti_3Al alloy has a hexagonal close-packed $D0_{19}$ structure and is characterized by space group 194 ($P6_3/mmc$), where aluminum and titanium atoms occupy $2c$ (1/3,2/3,1/4) and $6h$ (x,2x,1/4) sites with $x = -0.170$, according to the Wyckoff classification. The theoretical lattice parameters of the alloy are a = 5.736 Å and c = 4.639 Å. Based on convergence tests, the plane-wave cutoff energy was set at 550 eV and a Γ-centered $13 \times 13 \times 17$ k-point mesh was used in the primitive unit cell of the α_2-Ti_3Al alloy. The $(2 \times 2 \times 2)$ supercell (i.e., 64 atoms) with mesh of $5 \times 5 \times 7$ k-points was used to study the substitutional defect formation and the oxygen absorption. The full structural optimization scheme involving change in the atomic positions as well as in the cell shape and volume was applied. Convergence was considered to be achieved if the difference in total energies for the next two iterations did not exceed 10^{-5} eV. Atomic positions were relaxed using the conjugate gradient algorithm until the forces at the atoms were at most 10^{-3} eV/Å.

The oxygen absorption energy was calculated by the formula:

$$E_{\text{abs}} = -\left[E(\text{Ti}_3\text{Al} + \text{O}) - E(\text{Ti}_3\text{Al}) - \frac{1}{2}E(\text{O}_2) \right], \tag{1}$$

where $E(\text{Ti}_3\text{Al} + \text{O})$ and $E(\text{Ti}_3\text{Al})$ are the total energies of the alloy with and without oxygen, respectively, and $E(\text{O}_2)$ is the total energy of the oxygen molecule calculated in an empty

cell with sides of $12 \times 13 \times 14$ Å. Factor 1/2 corresponds to the absorption of one oxygen atom in the computational cell.

The formation energy of a substitutional defect was estimated by following equation:

$$E_f = E(\text{Ti}_3\text{Al} + \text{Imp}) - E(\text{Imp}) + E(\text{Ti}/\text{Al}) - E(\text{Ti}_3\text{Al}), \tag{2}$$

where $E(\text{Ti}_3\text{Al} + \text{Imp})$ and $E(\text{Ti}_3\text{Al})$ are the total energies of the alloy with and without impurity, respectively, and $E(\text{Ti}/\text{Al})$ and $E(\text{Imp})$ is the total energy of the titanium/aluminum (in dependence on occupied sublattice) and the impurity metal in the ground state per atom, respectively.

In accordance with the approach suggested by Lozovoi with co-authors [45] for embrittlement of grain boundaries, the effect of a substitutional (interstitial) defect on any physical quantity can be decomposed into three (two) contributions. In Figure 1a, several steps of the change in some physical quantity Z are shown. Following Lozovoi's notation, we will call the first step as "host removal" (*HR*), since it results in change in Z due to removal of a matrix atom, i.e., vacancy formation without optimization (system B in Figure 1a). The second step, "substitutional structure" (*SS*), is connected with a deformation of the undoped system with the unrelaxed vacancy so that the new structure corresponds to the doped structure with the unrelaxed vacancy (system C in Figure 1a). Finally, the value of Z is changed due to the impurity incorporation. The corresponding contribution we will call "chemical + compressed impurity" (*CC*). In Figure 1a, the undoped and doped systems are marked A and D, respectively.
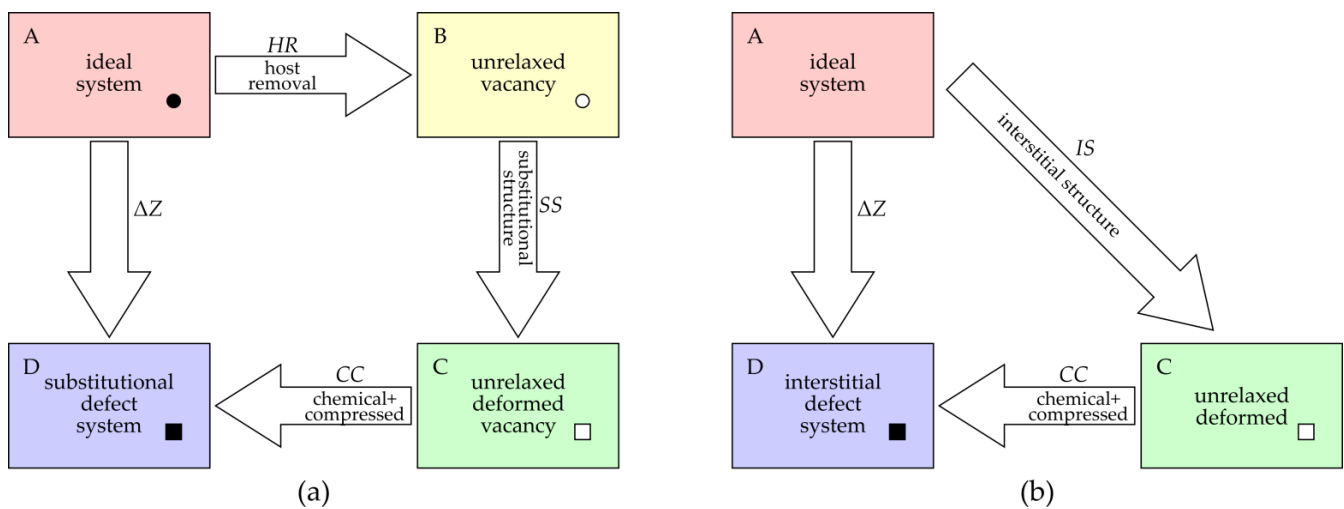

Figure 1. Schematic representation of influence of the substitutional (**a**) and interstitial (**b**) defect on a physical quantity Z. System A and D are fully relaxed ideal and defect supercells; B is created by substituting a host atom in A (black circle) with vacancies (white circle) without further relaxation; C is created by substituting an impurity atom in D (black square) with vacancies (white square) without further relaxation.

Summing up the above considerations, the contributions to ΔZ in the case of a substitutional impurity are:

$$HR = Z(\text{B}) - Z(\text{A}), \tag{3}$$

$$SS = Z(\text{C}) - Z(\text{B}), \tag{4}$$

$$CC = Z(\text{D}) - Z(\text{C}), \tag{5}$$

As a result, ΔZ can be expressed using Equations (3)–(5) as

$$\Delta Z = Z(\text{D}) - Z(\text{A}) = HR + SS + CC. \tag{6}$$

In the case of an interstitial impurity, the first (*HR*) and second (*SS*) stages should be replaced by a single "interstitial structure" (*IS*) (Figure 1b):

$$IC = Z(C) - Z(A), \tag{7}$$

and

$$\Delta Z = Z(D) - Z(A) = IC + CC. \tag{8}$$

The interaction energy between two atoms X and Y was calculated using following expression:

$$E_{\text{int}} = E(\text{Ti}_3\text{Al} + \text{X} + \text{Y}) - E(\text{Ti}_3\text{Al} + \text{X}) - E(\text{Ti}_3\text{Al} + \text{Y}) + E(\text{Ti}_3\text{Al}), \tag{9}$$

where $E(\text{Ti}_3\text{Al} + \text{X} + \text{Y})$, $E(\text{Ti}_3\text{Al} + \text{X})$, and $E(\text{Ti}_3\text{Al} + \text{Y})$ are the total energy of the Ti_3Al including both X and Y atoms, the X atom only, and the Y atom only, respectively, and $E(\text{Ti}_3\text{Al})$ is the total energy of the perfect host crystal. The positive value of E_{int} means that the interaction is repulsive, and negative means it is attractive. The larger the absolute value of E_{int}, the stronger is the interaction.

3. Results and Discussion

3.1. Substitutional Defect Formation

3.1.1. Single Impurity Atom

Figure 2 shows the calculated values of the substitutional defect formation energy for the Ti and Al sublattices in the case of elements of the VB–VIIB groups. It can be seen that all impurities prefer to occupy the Ti sublattice. This trend is in agreement with the results of earlier papers [33,35]. It should be noted that significant differences in specific values are due to the following factors: in [33], the chemical potential of Ti and Al was estimated based on thermodynamic equilibrium between the α_2-Ti_3Al and γ-TiAl alloys, while in [35], another approximation for the exchange-correlation potential was applied. The difference in the defect formation energy for the two sublattices reaches 0.7–2.0 eV (0.7–1.6 eV in [33,35]). This suggests that at moderate temperatures, all impurity atoms substitute for Ti with probability of ~100%. In this connection, further discussion is given only in case of impurities on the Ti sublattice.
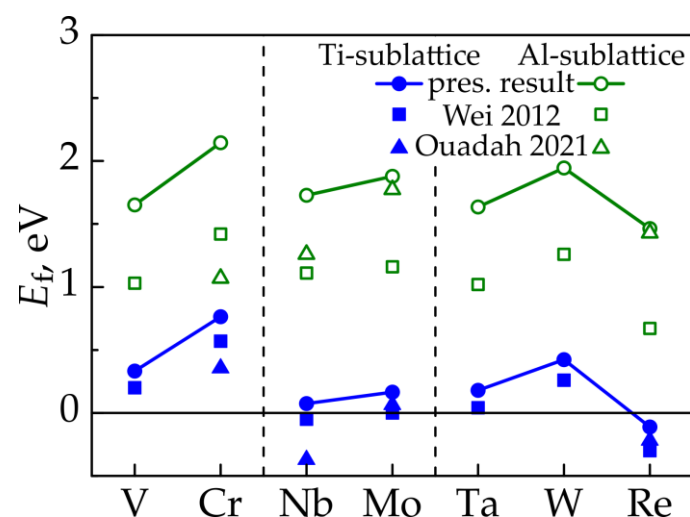

Figure 2. Formation energy (E_f) of the substitutional defect for both Ti and Al sublattice in comparison with results of Wei 2012 [33] and Ouadah 2021 [35].

The calculated values of the *HR*, *SS*, and *CC* contributions to the substitutional defect formation energy in accordance with Equations (3)–(5) are presented in Table 1. Note that the *SS* contribution can be considered as a mechanical one (μ), since it is due to the

difference in the size of the impurity and Ti atoms. It can be seen that this contribution is two orders of magnitude smaller than the contributions of the *HR* and *CC* mechanisms. Recall that the former one is associated with the breaking of chemical bonds when a titanium atom is removed, while the latter is associated with the formation of new impurity–matrix bonds. Therefore, the sum of *HR* and *CC* can be considered as a chemical contribution (χ) to the substitutional defect formation energy. Since *HR* does not depend on the impurity and represents the formation energy of the Ti vacancy without relaxation, it is convenient to use the chemical contribution χ alongside with the mechanical μ one in the further discussion. It is interesting that, taking into account the results of our earlier work [34], we can conclude that the relaxation energy of the α_2-Ti$_3$Al alloy to the energy of a vacancy is ~0.25 eV, which is an order of magnitude greater than the mechanical contribution μ during the formation of a substitutional defect. Thus, E_f is mainly determined by the difference in the binding energy between impurity–matrix and Ti–matrix, i.e., the chemical contribution (Figure 3). The cases of exception are Nb and Re impurities, since for them the χ and μ contributions are comparable.

Table 1. Formation energy of the substitutional defect in Ti sublattice (E_f), as well as the *HR*, *SS*, *CC* contributions.

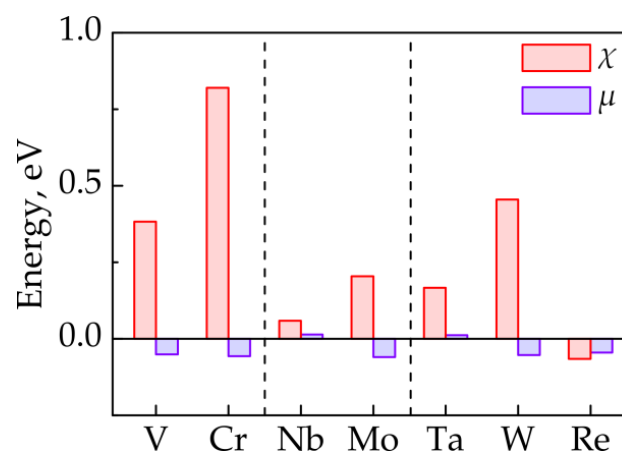| Impurity	E_f, eV	*HR*, eV	*SS* (μ), eV	*CC*, eV	χ, eV
V	0.332		−0.051	−2.073	0.383
Cr	0.763		−0.057	−1.635	0.820
Nb	0.075		0.014	−2.397	0.059
Mo	0.164	2.456	−0.040	−2.252	0.204
Ta	0.179		0.012	−2.288	0.167
W	0.422		−0.033	−2.001	0.455
Re	−0.111		−0.045	−2.521	−0.066
V	0.332		−0.051	−2.073	0.383

Figure 3. Both chemical (χ) and mechanical (μ) contributions to the defect formation energy.

Figure 4 shows the values of the contribution μ versus the difference (ΔR_{cov}) in covalent radii of impurity and titanium atoms [46]. It can be seen that μ is in good agreement with ΔR_{cov}, the correlation coefficient *R* is 0.88, and the standard deviation σ is 0.013 eV. At the same time, the chemical contribution is not only determined by the hybridization contribution, which can be estimated by calculating the Crystal Orbital Hamilton Populations (COHP) [47,48]. Note that the COHP curve integrated up to the Fermi level and, taken with the opposite sign (−ICOHP), can be considered as a measure of the hybridization contribution. Thus, as seen from Figure 5, the correlation between χ and the values of −ICOHP is weak enough: *R* equals −0.61 and σ = 0.216 eV. Unfortunately, it is quite difficult to estimate the metallic contribution to the chemical bonding, while the

ionic contribution should be insignificant, since the electronegativity of impurities differs slightly from that of titanium. For example, the maximum difference reaches 0.62 eV$^{1/2}$ in the case of Mo and for other metals it does not exceed 0.36 eV$^{1/2}$ [46].
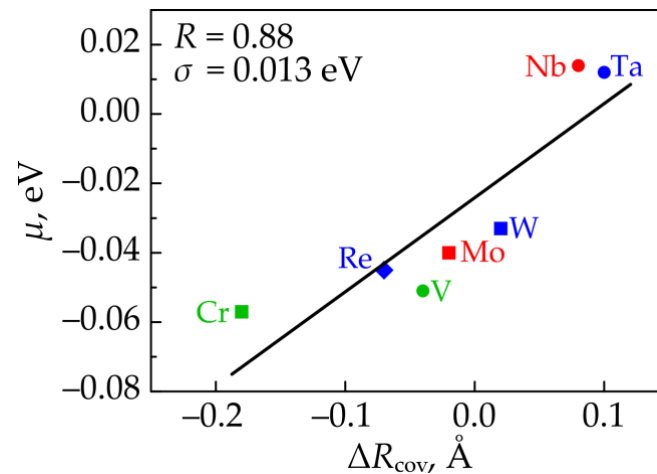

Figure 4. Correlation between mechanical contribution μ to the defect formation energy and difference in the covalent radii between impurity and Ti atoms. The solid lines are obtained by the least-squares method.
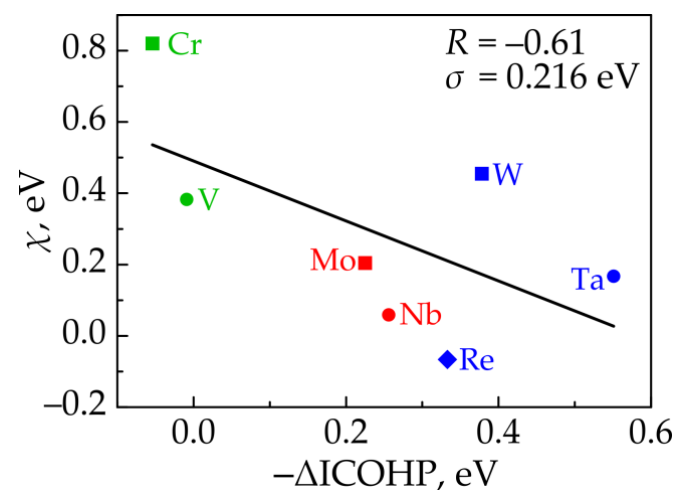

Figure 5. Correlation between chemical contribution χ to the defect formation energy and difference in ICOHP per bond between impurity–matrix and Ti–matrix bonds. The solid lines are obtained by the least-squares method.

3.1.2. Two Impurity Atoms

In the general case for a lattice with the hexagonal symmetry, the coordination ellipsoids should be considered instead of the coordination spheres [49]. In this regard, the nearest neighboring atoms (1NN) can be divided into two types: (i) atoms lying in the same (0001) plane as the selected atom (1_{in}) and (ii) atoms lying in neighboring planes (1_{out}, see Figure 6a). In both groups there are six neighboring atoms (Table 2). In the case of the second coordination ellipsoid (2NN), there are only six titanium atoms that lie in adjacent (0001) planes (Figure 6b). As seen from Figure 6c, two atoms located in the adjacent (0001) planes exactly above and below the selected atom are the third neighbors (3NN). Finally, in the case of the fourth coordination ellipsoid, the atomic distribution manner is similar to that in the first coordination ellipsoid: there are six atoms in the same (0001) plane (4_{in}) and twelve atoms in the adjacent (0001) planes (4_{out}) (Figure 6d). All data, including interatomic distances and multiplicities of atoms, are given in Table 2. Frankly speaking, since the value

of $2c/a = 1.617$ differed insignificantly from the value of 1.633 for an ideal HCP structure, the coordination ellipsoid is quite close to a sphere, and there is an insignificant difference in the distance to atoms 1_{in} and 1_{out} as well as 4_{in} and 4_{out}.
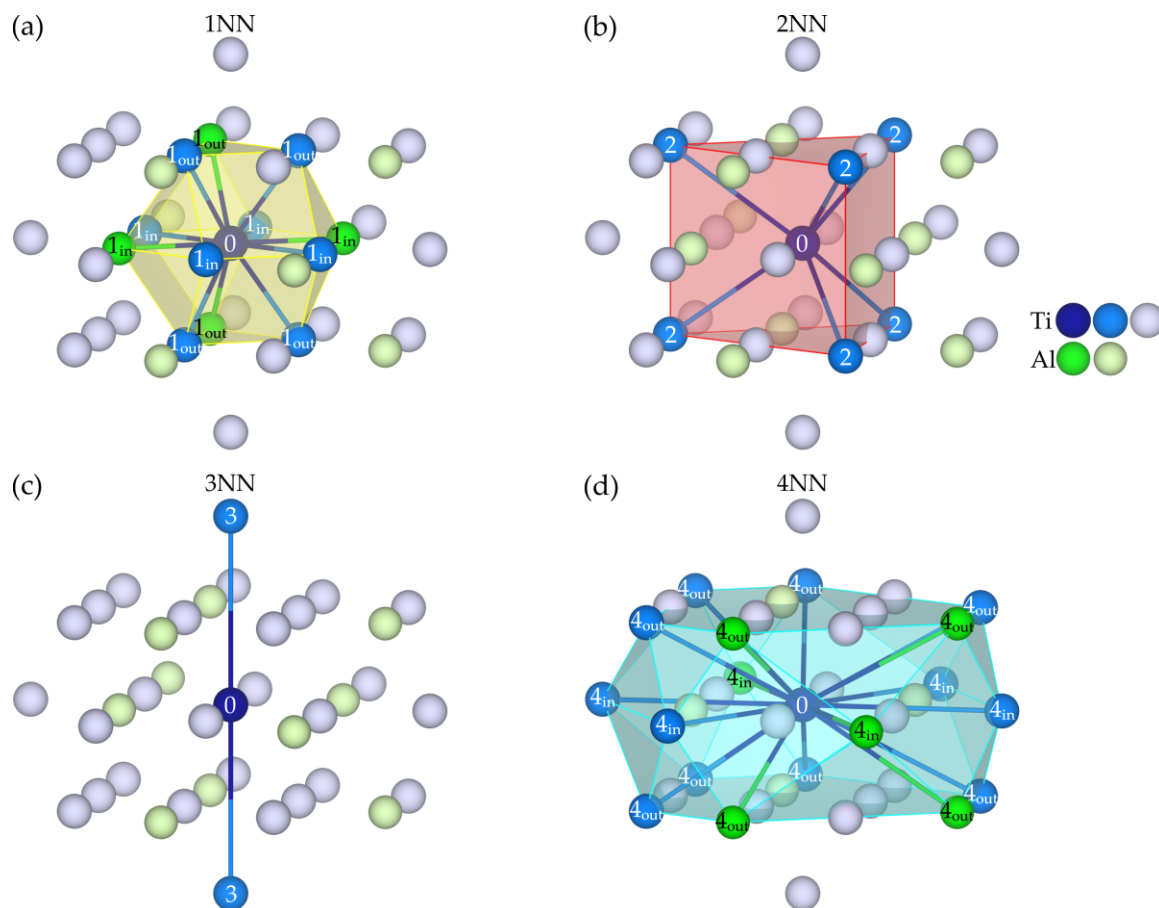

Figure 6. Considered coordination ellipsoids: the first (**a**), second (**b**), third (**c**), and fourth (**d**) ones.

Table 2. Interatomic distances and their multiplicities for the first four coordination ellipsoids.

Coordination Ellipsoid	Denotation of Atoms	d(Ti–Ti), Å	d(Ti–Al), Å
1NN	1_{in} 1_{out}	4×2.82 4×2.87	2×2.87 2×2.83
2NN	2	6×4.02	–
3NN	3	2×4.64	–
4NN	4_{in} 4_{out}	4×4.97 8×4.94	2×5.00 4×4.98

The interaction energy between impurity atoms E_{int} was estimated as a function of interatomic distance. Calculations showed that in the case of pairs of identical atoms, regardless of their combination, the lowest interaction energy corresponds to the situation when the impurity atoms are in the second neighbors relative to each other (Figure 7a). Moreover, only in the case of Mo, W, and Re is the interaction energy negative, which indicates an energetically preferable configuration of impurity atoms. The Cr, Nb, and Ta atoms prefer to be as far as possible from each other. A similar situation takes place in the case of pairs of different atoms (Figure 7b). The only exception is the Nb–Re pair, for which the interaction energy is negative. It is known that as the distance between atoms increases, the interaction energy should tend to zero. It can be seen from Figure 7 that, in

the case when the impurity atoms are the sixth neighbors of each other, the interaction energy becomes less than 0.02 eV.
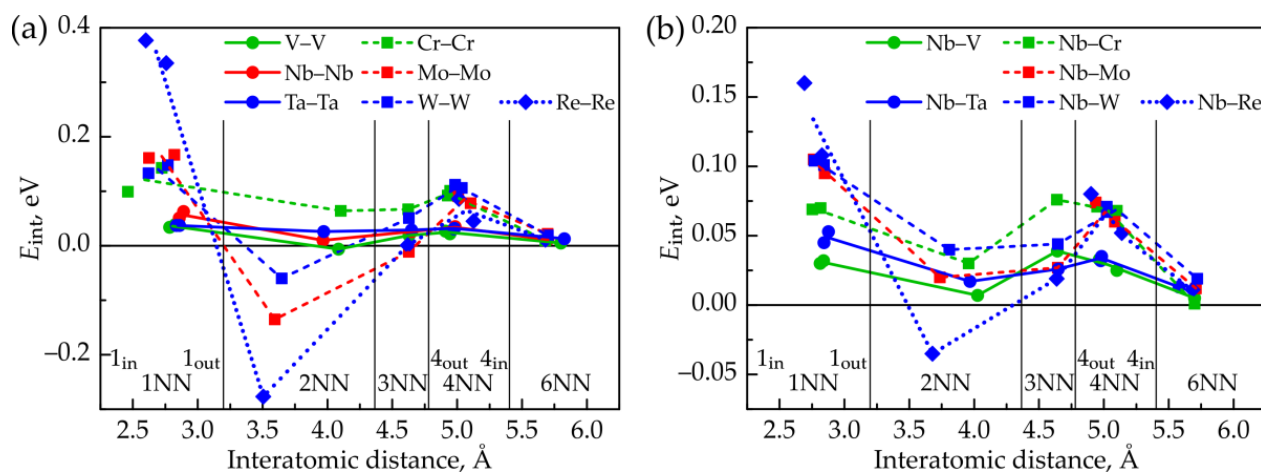

Figure 7. Interaction energy in pairs of identical (**a**) and different (**b**) impurity atoms depending on their interatomic distance. The polygonal chains are given according to the average values of energies and distances for each coordination ellipsoid.

Table 3 shows the calculated contributions to the interaction energy between impurity atoms at second neighbors' position. It can be seen that the mechanical and chemical contributions are comparable in magnitude. The negative values of E_{int} are found for V–V, Mo–Mo, W–W, Re–Re, and Nb–Re combinations. In the case of the Mo–Mo pair, both contributions are negative, the mechanical contribution is dominant for V–V, W–W, and Nb–Re, and the chemical one for Re–Re. In general, it can be seen from Table 3 that with an increase in the occupation of the impurity valence band the chemical contribution to the interaction energy increases in magnitude. The values of the correlation coefficient and the standard deviation are 0.78 and 0.037 eV, respectively. Thus, the dominance of the chemical contribution in the case of Re–Re can be explained by its high valence.

Table 3. Interaction energy (E_{int}) between impurity atoms at second neighbor positions, split into mechanical (μ) and chemical (χ) contributions.

Impurity	E_{int}, eV	μ, eV	χ, eV
V–V	−0.006	−0.008	0.002
Cr–Cr	0.064	0.011	0.052
Nb–Nb	0.010	0.005	0.005
Mo–Mo	−0.135	−0.056	−0.079
Ta–Ta	0.026	−0.015	0.041
W–W	−0.060	−0.056	−0.004
Re–Re	−0.277	−0.044	−0.233
Nb–V	0.007	−0.012	0.018
Nb–Cr	0.030	−0.038	0.068
Nb–Mo	0.020	−0.046	0.066
Nb–Ta	0.017	−0.004	0.021
Nb–W	0.040	−0.045	0.085
Nb–Re	−0.035	−0.085	0.050

3.2. Impurity Influence on the Oxygen Absorption

The highest energy of oxygen absorption was found to be in the octahedral Ti-rich site (2*a* Wyckoff position) that is in agreement with the results of earlier experimental [50] and theoretical [51,52] papers. The oxygen absorption energy in other positions (4*f*, 6*g*, 6*h*, for

details see [52]) is by 1.5–2.3 eV lower. The probability (p_i) of oxygen to be absorbed in a specific site i can be estimated according to the Boltzmann distribution as

$$p_i = \frac{n_i \exp(E_{\mathrm{abs}}(i)/k_{\mathrm{B}}T)}{\sum\limits_j n_j \exp(E_{\mathrm{abs}}(j)/k_{\mathrm{B}}T)}, \tag{10}$$

where $E_{\mathrm{abs}}(i)$ is the oxygen absorption energy in the site i, n_i is the multiplicity of position i within the primitive cell, k_{B} is the Boltzmann constant, and T is temperature; the summation is carried out over all absorption positions. Thus, at the moderate temperature all oxygen atoms should occupy 2a positions with 100% probability. Since there are only two 2a sites in the primitive cell of the alloy, the absorption in these sites is possible for an oxygen atom concentration of less than 25 at.%. Note that, in reality, this percentage is much lower due to the alloy oxidation accompanied by the formation of the titanium and aluminum oxides. In addition, the migration barrier from this position controls the oxygen diffusivity in the α_2-Ti$_3$Al alloy [38].

Since titanium has a high affinity for oxygen, the fact that all the considered impurities lead to a decrease in oxygen absorption energy is expected (Figure 8). In fact, the more distant from titanium the impurity element is in the periodic table, the stronger it lowers the oxygen absorption energy. It can be seen from Figure 8 that it is the chemical contribution that has the main effect. Even if some substituting atoms are smaller than titanium, the mechanical contribution is negative for all considered impurities. It results from the fact that the equilibrium length of the Me–O bond is larger than that of Ti–O. This explains the increase of μ (in magnitude) with the filling of the impurity d-shell.
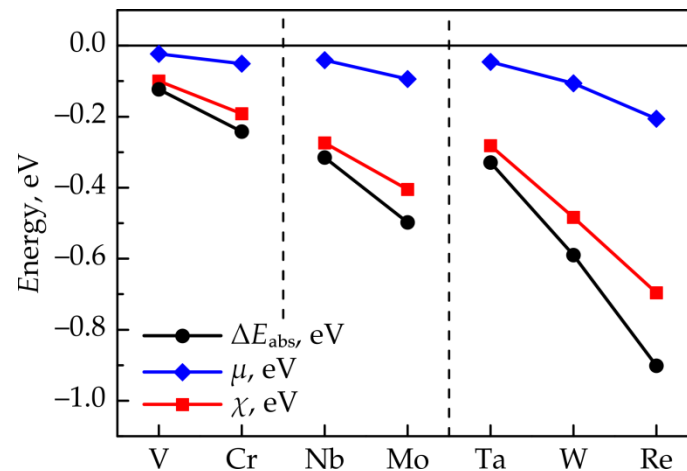

Figure 8. Change in the oxygen absorption energy due to doping (ΔE_{abs}) by a single atom, decomposed into mechanical (μ) and chemical (χ) contributions.

Taking into account the results from Section 3.1.2, the joint effect of two atoms will be considered in the second neighbor configuration. Obviously, the appearance of the second impurity atom near oxygen enhances the change in the absorption energy (Figure 9). The dominant factor responsible for a decrease in the oxygen absorption energy is the chemical contribution. The sum of values of ΔE_{abs} calculated for each atom separately (red and blue bars in Figure 9), shown by green diamonds in Figure 9, is quite close to the results of calculating ΔE_{abs} in the presence of two impurity atoms (yellow bars in Figure 9). The maximum difference between estimated $\Delta E_{\mathrm{abs}}(\mathrm{Imp1}) + \Delta E_{\mathrm{abs}}(\mathrm{Imp2})$ and ab initio calculated $\Delta E_{\mathrm{abs}}(\mathrm{Imp1} + \mathrm{Imp2})$ values is obtained for the Re–Re pair and it is equal to 0.11 eV. Denoting this difference ε,

$$\varepsilon = \Delta E_{\mathrm{abs}}(\mathrm{Imp1}) + \Delta E_{\mathrm{abs}}(\mathrm{Imp2}) - \Delta E_{\mathrm{abs}}(\mathrm{Imp1} + \mathrm{Imp2}). \tag{11}$$
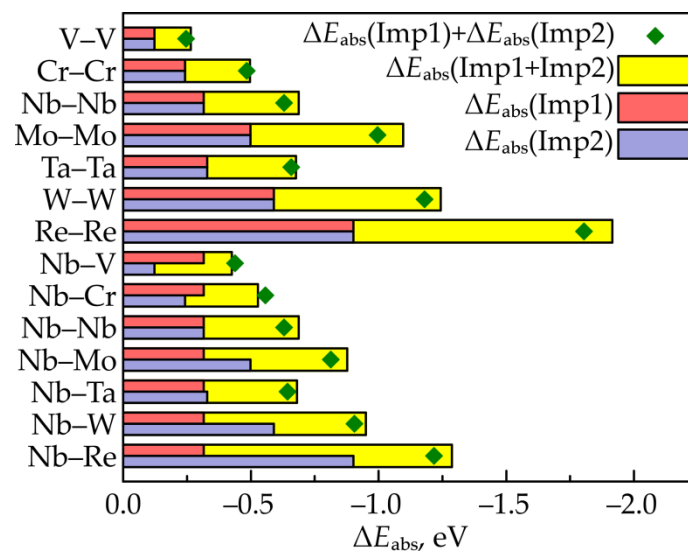
Figure 9. Change in the oxygen absorption energy due to alloying by one and two impurity atoms.

We suppose that the value of ε should be correlated with the interaction energy between impurity atoms. Due to the presence of oxygen, these interaction energies differ from those earlier calculated and given in Table 3. A sufficiently high electronegativity of oxygen leads to O–Me bonds being highly ionic. Therefore, impurity atoms get a charge of the same sign that leads to a repulsion interaction. As a result, the interaction energy becomes positive for all considered pairs of atoms, which leads to an additional decrease in the oxygen absorption energy. Indeed, this can be seen from Figure 10. In this case, the correlation coefficient between the interaction energy and the energy difference ε is -0.82, with the standard deviation of 0.022 eV. Considering just the effects of each impurity atom separately, the effect of two impurity atoms can be predicted as the sum of two corresponding contributions (Figure 11). In the case of such an estimation, the maximal error is 0.11 eV, and the relative error is less than 9%.
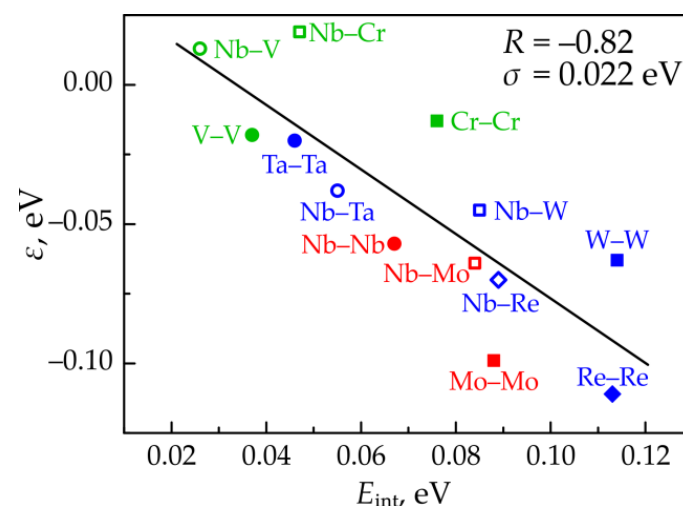

Figure 10. Correlation between ε and the interaction energy between impurity atoms in the presence of oxygen. The solid lines are obtained by the least-squares method.

Thus, in the case of an α_2-Ti$_3$Al alloy doped with elements of the VB–VIIB groups, with an increase in the impurity concentration or the addition of a second alloying element, the following conclusions can be drawn: (i) the configuration with the impurity atoms substituting for Ti, and being the second neighbors relative to each other, is the energy preferable one; (ii) the oxygen absorption energy is decreased for the positions near the

impurity and the effect becomes stronger with the filling of its *d*-shell; (iii) if oxygen locates in the region between impurity atoms, their effect is additively enhanced, which makes it possible to predict the joint effect of impurities with an accuracy of ~91%; (iv) regions near impurities can prevent the oxygen diffusion, since its penetration is energetically unfavorable. The latter is expected to be studied in more detail in our forthcoming papers.
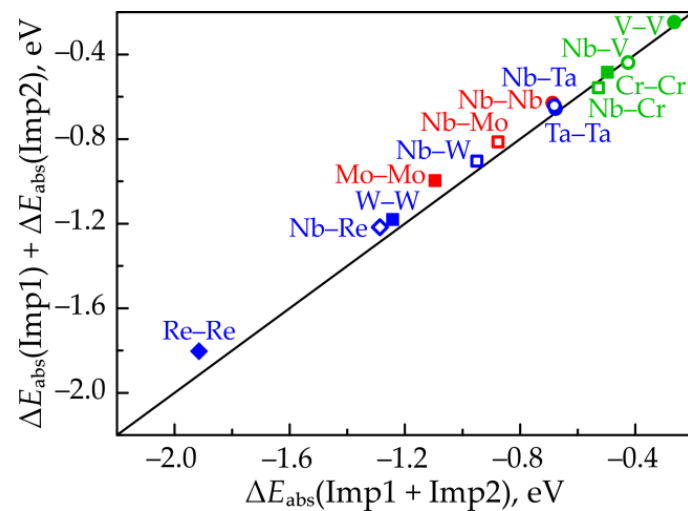

Figure 11. Comparison of $\Delta E_{abs}(\text{Imp1}) + \Delta E_{abs}(\text{Imp2})$ and $\Delta E_{abs}(\text{Imp1} + \text{Imp2})$ values.

Finally, several remarks should be made. First, the above-mentioned results are valid if impurity atoms can be freely placed in the first four coordination ellipsoids according to energy preference. This means that the total concentration of the impurities should not exceed ~5.3 at.% (2/38, where 38 is the total number of atoms in the first four coordination ellipsoids). Moreover, treatment can also have an influence on the distribution of the impurity atoms. Second, it is known that the α_2-Ti$_3$Al alloy can be disordered, transforming to α-structure. In this case, all obtained results remain valid, since a small amount of aluminum cannot block a coordination ellipsoid. Thirdly, a direct experimental confirmation of the established trends is quite difficult. Nevertheless, it can be done indirectly. For example, a more or less uniform distribution of Nb atoms in the alloy substrate was observed in [27], whereas Y atoms showed a tendency to form clusters. Such distribution of Nb agrees with our conclusion that Nb atoms prefer to be as far as possible from each other.

4. Conclusions

This manuscript is a theoretical study of the influence of the substitutional impurities of elements from the VB–VIIB groups, such as V, Cr, Nb, Mo, Ta, W, and Re, on the oxygen absorption in the intermetallic α_2-Ti$_3$Al alloy. It is shown that the substitution for a Ti atom by these impurities is more preferential in energy than substituting Al. In the former case, the defect formation energy spans the range from -0.11 to 0.76 eV, while in the latter case it is 1.46–2.15 eV. For both sublattices, the highest values of the defect formation energy correspond to chromium. It was found that this effect is mainly due to the chemical contribution to the substitutional defect formation energy. All considered, the impurities result in a decrease in the oxygen absorption energy. Moreover, it is the chemical contribution that is responsible for this effect.

The interaction energy between two impurity atoms was calculated as a function of their relative positions. It was shown that the structure with impurities as the second neighbors to each other is preferred one. At the same time, only for Mo–Mo, W–W, Re–Re, and Nb–Re pairs is this energy is negative. In other words, most of the impurity atoms considered prefer to be as far as possible from each other. The energy preference of the second neighbor configuration is conditioned by the mechanical contribution in the case of W–W and Nb–Re, by the chemical contribution for Re–Re, and both contributions in

the case of the Mo–Mo interaction. It was established that the effect of two impurity atoms on the oxygen absorption energy can be estimated as the sum of the effects of the separate impurities. Error in such estimation does not exceed 9%. The latter can be useful in modeling of effect of impurity combinations on the oxygen temperature-dependent diffusion coefficient.

References

1. Li, Z.; Gao, W. High temperature corrosion of intermetallics. In *Intermetallics Research Progress*; Berdovsky, N., Ed.; Nova Science: New York, NY, USA, 2008; pp. 1–64.
2. Zhang, T.; Fan, G.; Wu, H.; Cui, X.; Huang, M.; Miao, K.; Geng, L. Atomic-scale analysis of early-stage precipitation in Ti(Al,Si)$_3$ alloy. *Mater. Des.* **2017**, *134*, 244–249. [CrossRef]
3. Appel, F.; Paul, J.D.H.; Oehring, M. *Gamma Titanium Aluminide Alloys: Science and Technology*; Wiley-VCH: Weinheim, Germany, 2011; pp. 1–745. [CrossRef]
4. Lasalmonie, A. Intermetallics: Why is it so difficult to introduce them in gas turbine engines? *Intermetallics* **2006**, *14*, 1123–1129. [CrossRef]
5. Lin, H.; Liang, W.; Miao, Q.; Li, S.; Ding, Z.; Cui, S.; Yi, J.; Qi, Y.; Yang, Z.; Yu, H. Constructing self-supplying Al$_2$O$_3$-Y$_2$O$_3$ coating for the γ-TiAl alloy with enhanced oxidation protective ability. *Appl. Surf. Sci.* **2020**, *522*, 146439. [CrossRef]
6. Djanarthany, S.; Viala, J.C.; Bouix, J. An overview of monolithic titanium aluminides based on Ti$_3$Al and TiAl. *Mater. Chem. Phys.* **2001**, *72*, 301–319. [CrossRef]
7. Swadźba, R.; Laska, N.; Bauer, P.P.; Krztoń, H. Effect of pre-oxidation on cyclic oxidation resistance of γ-TiAl at 900 °C. *Corros. Sci.* **2020**, *177*, 108985. [CrossRef]
8. Wu, J.J.; Yan, H.J.; Cao, F.H.; Wu, L.K. Oxidation performance and interfacial reaction behavior of glass-ceramic coating on TiAl alloy with electrodeposited SiO$_2$ interlayer. *Surf. Coat. Technol.* **2010**, *422*, 127495. [CrossRef]
9. Leyens, C.; Peters, M. *Titanium and Titanium Alloys: Fundamentals and Applications*; Wiley-VCH: Weinheim, Germany, 2003; pp. 1–513. [CrossRef]
10. Umakoshi, Y.; Yamaguchi, M.; Sakagami, T.; Yamane, T. Oxidation resistance of intermetallic compounds Al$_3$Ti and TiAl. *J. Mater. Sci.* **1989**, *24*, 1599–1603. [CrossRef]
11. Becker, S.; Rahmel, A.; Schorr, M.; Schütze, M. Mechanism of isothermal oxidation of the intermetallic TiAl and of TiAl alloys. *Oxid. Met.* **1992**, *38*, 425–464. [CrossRef]
12. Maurice, V.; Despert, G.; Zanna, S.; Josso, P.; Bacos, M.P.; Marcus, P. XPS study of the initial stages of oxidation of α$_2$-Ti$_3$Al and γ-TiAl intermetallic alloys. *Acta Mater.* **2007**, *55*, 3315–3325. [CrossRef]
13. Wu, L.K.; Wu, W.Y.; Song, J.L.; Hou, G.Y.; Cao, H.Z.; Tang, Y.P.; Zheng, G.Q. Enhanced high temperature oxidation resistance for γ-TiAl alloy with electrodeposited SiO$_2$ film. *Corros. Sci.* **2018**, *140*, 388–401. [CrossRef]
14. Qu, S.J.; Tang, S.Q.; Feng, A.H.; Feng, C.; Shen, J.; Chen, D.L. Microstructural evolution and high-temperature oxidation mechanisms of a titanium aluminide based alloy. *Acta Mater.* **2018**, *148*, 300–310. [CrossRef]
15. Bartholomeusz, M.F.; Wert, J.A. The effect of thermal exposure on microstructural stability and creep resistance of a two-phase TiAl/Ti$_3$Al lamellar alloy. *Metall. Mater. Trans. A* **1994**, *25*, 2371–2381. [CrossRef]
16. Kishida, K.; Inui, H.; Yamaguchi, M. Deformation of lamellar structure in TiAl–Ti$_3$Al two-phase alloys. *Philos. Mag. A* **1998**, *78*, 1–28. [CrossRef]
17. Yamaguchi, M.; Inui, H.; Ito, K. High-temperature structural intermetallics. *Acta Mater.* **2000**, *48*, 307–322. [CrossRef]
18. Kartavykh, A.V.; Kaloshkin, S.D.; Cherdyntsev, V.V.; Gorshenkov, M.V.; Sviridova, T.A.; Borisova, Y.V.; Senatov, F.S.; Maksimkin, A.V. Application of microstructured intermetallides in turbine manufacture. Part 2: Problems in development of heat-resistant alloys based on TiAl (A review). *Inorg. Mater. Appl. Res.* **2013**, *4*, 36–45. [CrossRef]

19. Bartholomeusz, M.F.; Yang, Q.; Wert, J.A. Creep deformation of a two-phase TiAl/Ti$_3$Al lamellar alloy and the individual TiAl and Ti$_3$Al constituent phases. *Scripta Metall. Mater.* **1993**, *29*, 389–394. [CrossRef]

20. Bartholomeusz, M.F.; Wert, J.A. Modeling creep deformation of a two-phase TiAl/Ti$_3$Al alloy with a lamellar microstructure. *Metall. Mater. Trans. A* **1994**, *25*, 2161–2171. [CrossRef]

21. Hsiung, L.M.; Nieh, T.G.; Choi, B.W.; Wadsworth, J. Interfacial dislocations and deformation twinning in fully lamellar TiAl. *Mater. Sci. Eng. A* **2002**, *329–331*, 637–643. [CrossRef]

22. Yang, H.S.; Jin, P.; Dalder, E.; Mukherjee, A.K. Superplasticity in a Ti$_3$Al-base alloy stabilized by Nb, V and Mo. *Scripta Metall. Mater.* **1991**, *25*, 1223–1228. [CrossRef]

23. Cheng, T.T.; Willis, M.R.; Jones, I.P. Effects of major alloying additions on the microstructure and mechanical properties of γ-TiAl. *Intermetallics* **1999**, *7*, 89–99. [CrossRef]

24. Mao, Y.; Li, S.; Zhang, J.; Peng, J.; Zou, D.; Zhong, Z. Microstructure and tensile properties of orthorhombic Ti–Al–Nb–Ta alloys. *Intermetallics* **2000**, *8*, 659–662. [CrossRef]

25. Muto, S.; Yamanaka, T.; Johnson, D.R.; Inui, H.; Yamaguchi, M. Effects of refractory metals on microstructure and mechanical properties of directionally-solidified TiAl alloys. *Mater. Sci. Eng. A* **2002**, *329–331*, 424–429. [CrossRef]

26. Mizuhara, Y.; Hashimoto, K.; Masahashi, N. Microstructure and phase stability of TiAl–W ternary alloy. *Intermetallics* **2003**, *11*, 807–816. [CrossRef]

27. Koo, C.H.; Evans, J.W.; Song, K.Y.; Yu, T.H. High-temperature oxidation of Ti$_3$Al–Nb alloys. *Oxid. Met.* **1994**, *42*, 529–544. [CrossRef]

28. Shida, Y.; Anada, H. Role of W, Mo, Nb and Si on oxidation of TiAl in air at high temperatures. *Mater. Trans. JIM* **1994**, *35*, 623–631. [CrossRef]

29. Kim, B.G.; Kim, G.M.; Kim, C.J. Oxidation behavior of TiAl-X (X=Cr, V, Si, Mo or Nb) intermetallics at elevated temperature. *Scripta Metall. Mater.* **1995**, *33*, 1117–1125. [CrossRef]

30. Okafor, I.C.I.; Reddy, R.G. The oxidation behavior of high-temperature aluminides. *JOM* **1999**, *51*, 35–40. [CrossRef]

31. Reddy, R.G.; Li, Y.; Arenas, M.F. Oxidation of a ternary Ti$_3$Al-Ta alloy. *High. Temp. Mater. Processes* **2002**, *21*, 195–205. [CrossRef]

32. Hao, Y.L.; Xu, D.S.; Cui, Y.Y.; Yang, R.; Li, D. The site occupancies of alloying elements in TiAl and Ti$_3$Al alloys. *Acta mater.* **1999**, *47*, 1129–1139. [CrossRef]

33. Wei, Y.; Zhang, Y.; Lu, G.H.; Xu, H. Effects of transition metals in a binary-phase TiAl–Ti$_3$Al alloy: From site occupancy, interfacial energetics to mechanical properties. *Intermetallics* **2012**, *31*, 105–113. [CrossRef]

34. Bakulin, A.V.; Kulkova, S.E. Effect of impurities on the formation energy of point defects in the γ-TiAl alloy. *J. Exp. Theor. Phys.* **2018**, *127*, 1046–1058. [CrossRef]

35. Ouadah, O.; Merad, G.; Abdelkader, H.S. Atomistic modelling of the γ-TiAl/α$_2$-Ti$_3$Al interfacial properties affected by solutes. *Mater. Chem. Phys.* **2021**, *257*, 123434. [CrossRef]

36. Kulkova, S.E.; Bakulin, A.V.; Kulkov, S.S. First-principles calculations of oxygen diffusion in Ti-Al alloys. *Latv. J. Phys. Tech. Sci.* **2018**, *6*, 20–29. [CrossRef]

37. Bakulin, A.V.; Kulkov, S.S.; Kulkova, S.E. Diffusion properties of oxygen in the γ-TiAl alloy. *J. Exp. Theor. Phys.* **2020**, *130*, 579–590. [CrossRef]

38. Bakulin, A.V.; Kulkov, S.S.; Kulkova, S.E. Diffusion properties of oxygen in the α$_2$-Ti$_3$Al alloy. *Intermetallics* **2021**, *137*, 107281. [CrossRef]

39. Blöchl, P.E. Projector augmented-wave method. *Phys. Rev. B* **1994**, *50*, 17953–17979. [CrossRef]

40. Kresse, G.; Joubert, J. From ultrasoft pseudopotentials to the projector augmented-wave method. *Phys. Rev. B* **1999**, *59*, 1758–1775. [CrossRef]

41. Kresse, G.; Hafner, J. Ab initio molecular dynamics for liquid metals. *Phys. Rev. B* **1993**, *47*, 558–561. [CrossRef]

42. Kresse, G.; Furthmüller, J. Efficiency of ab-initio total energy calculations for metals and semiconductors using a plane-wave basis set. *Comput. Mater. Sci.* **1996**, *6*, 15–50. [CrossRef]

43. Kresse, G.; Furthmüller, J. Efficient iterative schemes for ab initio total-energy calculations using a plane-wave basis set. *Phys. Rev. B* **1996**, *54*, 11169–11186. [CrossRef]

44. Perdew, J.P.; Burke, K.; Ernzerhof, M. Generalized gradient approximation made simple. *Phys. Rev. Lett.* **1996**, *77*, 3865–3868. [CrossRef]

45. Lozovoi, A.Y.; Paxton, A.T.; Finnis, M.W. Structural and chemical embrittlement of grain boundaries by impurities: A general theory and first-principles calculations for copper. *Phys. Rev. B* **2006**, *74*, 155416. [CrossRef]

46. Haynes, W.M. *CRC Handbook of Chemistry and Physics*, 96th ed.; Internet Version 2016; CRC Press: Raton, FL, USA; Taylor and Francis: Raton, FL, USA, 2015–2016; pp. 1–3020.

47. Dronskowski, R.; Blöchl, P.E. Crystal orbital Hamilton populations (COHP): Energy-resolved visualization of chemical bonding in solids based on density-functional calculations. *J. Phys. Chem.* **1993**, *97*, 8617–8624. [CrossRef]

48. Maintz, S.; Deringer, V.L.; Tchougreeff, A.L.; Dronskowski, R. LOBSTER: A tool to extract chemical bonding from plane-wave based DFT. *J. Comput. Chem.* **2016**, *37*, 1030–1035. [CrossRef]

49. Podolskaya, E.A.; Krivtsov, A.M. Description of the geometry of crystals with a hexagonal close-packed structure based on pair interaction potentials. *Phys. Solid State* **2012**, *54*, 1408–1416. [CrossRef]

50. Jones, C.Y.; Luecke, W.E.; Copland, E. Neutron diffraction study of oxygen dissolution in α_2-Ti$_3$Al. *Intermetallics* **2006**, *14*, 54–60. [CrossRef]

51. Wei, Y.; Zhou, H.B.; Zhang, Y.; Lu, G.H.; Xu, H. Effects of O in a binary-phase TiAl–Ti$_3$Al alloy: From site occupancy to interfacial energetics. *J. Phys. Condens. Matter* **2011**, *23*, 225504. [CrossRef]

52. Bakulin, A.V.; Latyshev, A.M.; Kulkova, S.E. Absorption and diffusion of oxygen in the Ti$_3$Al alloy. *J. Exp. Theor. Phys.* **2017**, *125*, 138–147. [CrossRef]